Applied Surface Science 258 (2011) 1711–1718

Contents lists available at SciVerse ScienceDirect

Applied Surface Science

journal homepage: www.elsevier.com/locate/apsusc

Albumin adsorption on oxide thin films studied by spectroscopic ellipsometry

P. Silva-Bermudez[a,b,*], S.E. Rodil[a], S. Muhl[a]

[a] Instituto de Investigaciones en Materiales, Universidad Nacional Autónoma de México, Circuito Exterior s/n, C.U., 04510, México D.F., Mexico
[b] Unidad de Posgrado, Facultad de Odontología, Universidad Nacional Autónoma de México, CU, 04510, México D.F., Mexico

ARTICLE INFO

Article history:
Received 18 July 2011
Received in revised form 9 September 2011
Accepted 5 October 2011
Available online 15 October 2011

Keywords:
Protein adsorption
Ellipsometry
Metal oxide thin film
Albumin

ABSTRACT

Thin films of tantalum, niobium, zirconium and titanium oxides were deposited by reactive magnetron sputtering and their wettability and surface energy, optical properties, roughness, chemical composition and microstructure were characterized using contact angle measurements, spectroscopic ellipsometry, profilometry, X-ray photoelectron spectroscopy and X-ray diffraction, respectively. The purpose of the work was to correlate the surface properties of the films to the Bovine Serum Albumin (BSA) adsorption, as a first step into the development of an initial in vitro test of the films biocompatibility, based on standardized protein adsorption essays. The films were immersed into BSA solutions with different protein concentrations and protein adsorption was monitored in situ by dynamic ellipsometry; the adsorption-rate was dependent on the solution concentration and the immersion time. The overall BSA adsorption was studied in situ using spectroscopic ellipsometry and it was found to be influenced by the wettability of the films; larger BSA adsorption occurred on the more hydrophobic surface, the ZrO_2 film. On the Ta_2O_5, Nb_2O_5 and TiO_2 films, hydrophilic surfaces, the overall BSA adsorption increased with the surface roughness or the polar component of the surface energy.

1. Introduction

The oxides of transition metals, such as Nb, Ta, Zr and Ti constitute an interesting group of materials with potential applications as biomaterials for orthopedic and dental implants. In the last ten years several reports have been published about new biomaterials based on these oxides, showing that these materials exhibit similar or even enhanced properties than those of standard biomaterials used in orthopedic and dental implants [1–6]. The majority of the studies have explored the biocompatibility of the oxides in vitro using cell lines or in vivo by implantation into animals; although the results are encouraging almost no information about the physicochemical properties of the materials which drive or influence their biocompatibility can be obtained. A deeper understanding of those physicochemical properties and the basic principles of the complex material–biological media interaction is required in order to obtain the ability to design novel biomaterials [7–10].

Whenever a foreign material comes in close contact with blood or physiological fluids one of the first process to occur is the adsorption of proteins on the material's surface; the conformation and profile of the adsorbed proteins control the subsequent biological processes and consequently greatly determine the biological response to the material [9,11,12].

In the present work, the adsorption of Bovine Serum Albumin (BSA) onto Ta, Nb, Zr and Ti oxide thin films, which are proposed as surface modifications for materials with potential biomedical applications, were studied by spectroscopic and dynamic ellipsometry. The aim of the work was to assess the influence of the physicochemical properties of the oxide thin films in the surface adsorption of BSA; to start acquiring the necessary knowledge and understanding of the correlations between surface physichochemical properties and protein adsorption to develop an initial in vitro biocompatibility test based on protein adsorption. Bovine Serum Albumin is a small (66 kDa, 14 nm × 4 nm × 4 nm) soft protein that was chosen as a model protein because its high abundance in blood plasma and because it readily adsorbs onto foreign surfaces dominating the first stages of protein adsorption [13,14].

2. Experimental details

2.1. Thin films deposition

The metal oxide thin films, tantalum oxide (TaO_x), niobium oxide (NbO_x), zirconium oxide (ZrO_x) and titanium oxide (TiO_x), were deposited under an Ar/O_2 atmosphere on Si(1 0 0) wafers by reactive radio frequency (RF) Balanced Magnetron Sputtering of metal targets; Ti, Ta, Nb or Zr (99.95% purity). The base pressure in the sputtering chamber was 4.33×10^{-4} Pa and during deposition

* Corresponding author at: Instituto de Investigaciones en Materiales, Universidad Nacional Autónoma de México, Circuito Exterior s/n, C.U., 04510, México D.F., Mexico. Tel.: +52 55 56224734; fax: +52 55 56161251.
E-mail address: suriel21@yahoo.com (P. Silva-Bermudez).

0169-4332/$ – see front matter © 2011 Elsevier B.V. All rights reserved.
doi:10.1016/j.apsusc.2011.10.020

the total pressure was 4 Pa using a gas composition of 80% Ar and 20% O_2. The incident RF power into the target was 200 W, the deposition time was 30 min and substrate–target distance was 4.5 cm. It is important to mention that no substrate heating was applied, since it was not intended to obtain crystalline but amorphous oxides.

2.2. Thin films characterization

The chemical composition of the films was characterized by X-ray Photoelectron Spectroscopy (XPS) using a commercial XPS VG Microtech Multilab ESCA 2000 with a CLAM MCD detector, Al K_α ($h\nu$ = 1453.6 eV) radiation, operating at 8×10^{-7} Pa, using a 500 μm spatial resolution and 50 and 20 eV pass energy for the acquisition of the survey and high resolution spectra, respectively. Curve fitting of the high resolution XPS spectra acquired in the regions of the C1s and O1s photoelectron peaks and the Ta4d, Nb3d, Ti2p and Zr3d photoelectron peaks, respectively for the different metal oxide films, were performed in the SDPv4.1 software® to obtain the elemental chemical composition. The films were also characterized by X-ray Diffraction (XRD) using a Bruker D8 XRD system in the Bragg–Bretano mode and monochromatized CuKα radiation. The Root Mean Square roughness (RMS), average roughness (R_a) and thickness of the films were evaluated using a Profilometer DEKTAK II; 10 and 20 measurements were averaged for the thickness and RMS and R_a values reported, respectively.

The surface energy and wettability of the films were obtained by contact angle measurements at room temperature (RT) in static sessile drop mode using a Ramé-Hart Inc. Goniometer coupled to a CCD Rainbow video camera. Double distilled water, formamide, diiodomethane and dimethyl sulfoxide were used as probe liquids and uniform 4 μL drops of the probe liquids were used for the acquisition of the contact angles, averaging 12 measurements of each liquid for the statistical analysis. The contact angles were determined using the Drop Snake software [15] and the total surface energy, $\gamma^{LW/AB}$, calculations were done according to the van Oss, Good and Chaudury LW/AB method [16].

Optical characterization of the thin films was done by means of spectroscopic ellipsometry (SE) using a Jobin Yvon Uvisel DH10 ellipsometer. Spectra were acquired from 1.5 to 5 eV at an angle of incidence (AOI) of 70° at room temperature inside an empty ellipsometric liquid cell to include any possible effect of the cell windows to first order in the interpretation of the acquired spectra. Optical properties and thicknesses of the thin films were obtained using the DeltaPsi2 software® to fit the experimental spectra using a four-phase optical model: (1) a crystalline Si layer as the substrate; (2) the metal oxide film modeled as one optical layer (OL) for TaO_x and NbO_x and two OL with variable void percentage for ZrO_x and TiO_x due to their density inhomogeneity [17–19]; (3) an interfacial layer modeled using a Bruggeman Effective Medium approximation to take into account the surface roughness and (4) air as the ambient. The OL representing the metal oxide films were parameterized using the Tauc–Lorentz dispersion formula. The pertinence of the optical models were verified by comparison of the refractive indices and band gaps obtained to values reported in the literature for similar films [17–21] and by corroboration of correspondence between the thickness obtained by SE and by profilometry. The χ^2 value was used as a figure of merit to evaluate the quality of the SE data fitting.

2.3. BSA adsorption

Lyophilized BSA (Sigma–Aldrich, A1933) was dissolved in phosphate buffer saline (PBS) 0.01 M, pH = 7.4, to obtain two stock solutions with protein concentrations of 1 mg/mL (BSA1) and 0.1 mg/mL (BSA0.1). Fresh solutions were prepared right before each adsorption experiment. Optical characterization of the BSA solutions was obtained using SE. The acquired spectra were fitted to a two-phase optical model using a transparent Cauchy model to obtain the refractive index of the solution, n_m. Pertinence of measurements was corroborated by comparison of the n_m obtained to refractive indices previously reported for albumin solutions [22,23].

For protein adsorption, the liquid ellipsometric cell was filled up with 12 mL of BSA solution and then the metal oxide film was immersed into the solution. Immediately after immersion, an ellipsometric dynamic routine was started acquiring a set of ellipsometric angles, Ψ and Δ, every 2 sec at 70° of AOI at a fixed energy of 3 eV. After 2400 s of immersion, an ellipsometry spectrum was acquired in situ at AOI of 70° from 1.5 to 4.2 eV; above this energy the signal intensity was too low to be detected. The refractive index, n_p, and thickness, d_p, of the adsorbed BSA layer were obtained by fitting the acquired spectrum to a four phase-optical model: (1) crystalline Si as the substrate; (2) the metal oxide film; (3) the adsorbed BSA layer and (4) the medium: BSA solution. The optical properties of the adsorbed BSA layer were parameterized using a transparent Cauchy model. The χ^2 value was used as a figure of merit to evaluate the quality of the SE data fitting. The surface mass concentration of the BSA layer, Γ, was then calculated according to the De Feijter's formula [24], using a value of 0.18 mg/mL for $\delta n/\delta C$ and the n_p and n_m calculated previously at 2 eV.

Table 1
Elemental composition of the metal oxide films.

Film	Elemental composition (at.%)			
	C	$O^{(O-C)}$	$O^{(O-M)}$	Metal
TaO_x	43.9	7.8	34.4	13.8
NbO_x	32	7.8	42.9	17.3
ZrO_x	44.8	5.7	33	16.5
TiO_x	27.9	9.2	42	20.9

O–C, oxygen bound to carbon; O–M, oxygen bound to metal.

3. Results

3.1. Film characterization

The XPS survey spectra of the TiO_x, NbO_x, TaO_x and ZrO_x films are shown in Fig. 1, where the only observable photoelectron peaks correspond to oxygen, the metal element in the film and spurious carbon due to film exposure to the atmosphere. The elemental composition obtained from the XPS results are presented in Table 1; all the films have a chemical composition equivalent to its most stable

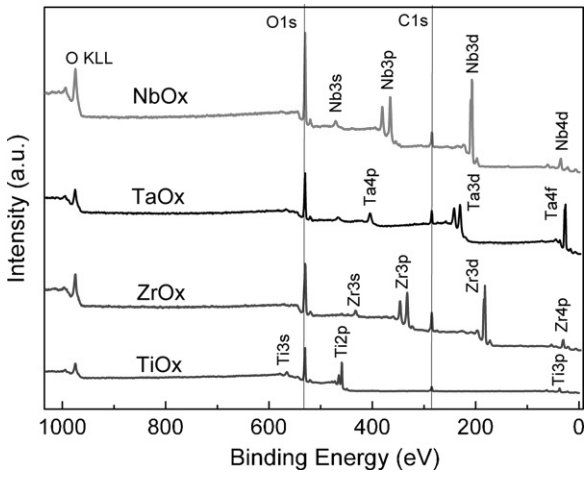

Fig. 1. XPS survey spectra of the deposited NbO_x, TaO_x, ZrO_x and TiO_x films.

Table 2
Thickness, R_a and RMS roughness of the metal oxide films.

Film	Thickness (nm)	R_a (nm)	RMS (nm)
TaO_x	270 ± 30	9.1 ± 0.5	11.5 ± 0.9
NbO_x	250 ± 24	7.5 ± 1.3	9.3 ± 1.5
ZrO_x	194 ± 15	5.9 ± 1.2	6.9 ± 1.3
TiO_x	54 ± 8	6.9 ± 0.8	8.2 ± 0.9

Table 3
Water contact angle (θ_w) and total surface energy parameters of the metal oxide films.

Film	θ_w (°)	$\gamma^{LW/AB}$ (mJ/m^2)	γ^{LW} (mJ/m^2)	γ^{AB} (mJ/m^2)
TaO_x	60 ± 1.8	45.5 ± 0.4	27.9 ± 6.6	17.6 ± 6.2
NbO_x	72 ± 1.8	44.4 ± 0.1	39.5 ± 1.2	5.96 ± 1.3
ZrO_x	82 ± 2.7	40.8 ± 0.3	38.1 ± 0.4	2.76 ± 0.1
TiO_x	74 ± 2.5	44.1 ± 0.1	38.9 ± 1.6	5.14 ± 1.6

stoichiometric oxide, i.e. Nb_2O_5, Ta_2O_5, TiO_2 and ZrO_2. The absence of any XPS peak corresponding to the Si(1 0 0) substrate indicated deposition of a uniform film in all cases.

The XRD patterns of the films are shown in Fig. 2. The patterns of the TiO_x, TaO_x and NbO_x films show no diffraction peaks, other than the Si(1 0 0) diffraction peak from the substrate; however, the pattern of the ZrO_x film showed two diffraction peaks corresponding to the ZrO_2 Baddeleyite phase, even though no crystalline structure was expected. The broadness of the Baddeleyite diffraction peaks implies nanometer size grains smaller than ≈5 nm.

The films thickness, R_a and RMS are shown in Table 2. The RMS values are significantly different ($p < 0.15$) among the different metal oxide films and varied from 6.9 nm for ZrO_x to 11.5 nm for TaO_x. The RMS and R_a values of the films are comparable to the spatial dimensions of the BSA molecule, 14 nm × 4 nm × 4 nm.

The values of the water contact angle, θ_w, and total surface energy parameters of the films are shown in Table 3. The θ_w values increased from TaO_x with $\theta_w = 60 \pm 1.8°$ towards NbO_x, TiO_x and ZrO_x with $\theta_w = 82 \pm 2.7°$. The TaO_x, NbO_x and TiO_x films had similar $\gamma^{LW/AB}$ values in the range between 44 and 45 mJ/m^2, while ZrO_x displayed a slightly lower $\gamma^{LW/AB}$, 40.8 mJ/m^2. The total surface energy can be considered as the contribution of two components, the polar, γ^{AB}, and the apolar, γ^{LW}, components. The TaO_x film showed the highest γ^{AB} value, 17.58 mJ/m^2, and it decreased towards NbO_x, TiO_x and ZrO_x down to $\gamma^{AB} = 2.77$ mJ/m^2.

The results obtained from the optical characterization of the films are summarized in Table 4, where the energy band gap, E_g,

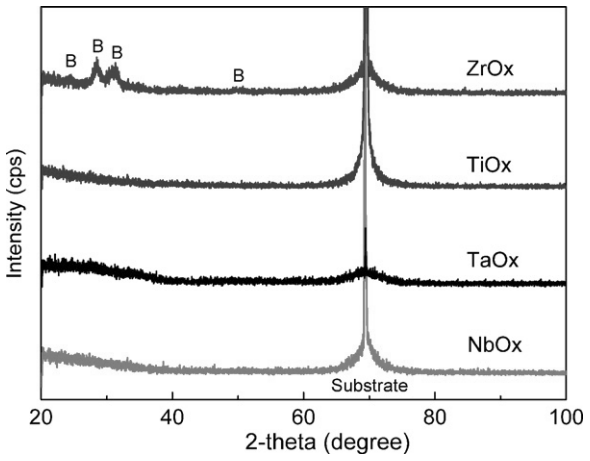

Fig. 2. XRD pattern of the deposited NbO_x, TaO_x, TiO_x and ZrO_x films. B corresponds to ZrO_2 Baddeleyite phase diffraction peaks. The Si(1 0 0) diffraction peak arising from the substrate where films were deposited is marked.

Table 4
Optical properties and thickness of the metal oxide films calculated from SE data acquisition and χ^2 obtained for fitting of the ellipsometry spectra.

Film	E_g (eV)	ε^∞	Thickness (nm)	χ^2
TaO_x	4.1 ± 0.04	1.8 ± 0.2	306 ± 8	7.2 ± 0.3
NbO_x	3.4 ± 0.03	1.9 ± 0.5	251 ± 9	9.9 ± 1.5
ZrO_x	2.9 ± 0.10	1.8 ± 0.4	197 ± 10	0.89 ± 0.1
TiO_x	3.2 ± 0.02	2.7 ± 0.2	58 ± 2	3.48 ± 0.2

the dielectric constant for high frequencies, ε^∞, the film thickness, the refractive index at 2 eV and the χ^2 obtained by SE are shown. The higher χ^2 values corresponded to the films for which more interference bands were obtained.

3.2. Protein adsorption

Representative examples of the ellipsometric dynamic data acquired during film immersion in BSA1 are shown in Fig. 3(a)–(d). The evolution of the BSA adsorption rate over time was similar for all the metal oxide films; a fast change-rate in Ψ and Δ occurred during the first 120 s of immersion and then the change-rate rapidly decreased, reaching quite a slow regime after approximately 1800 s. In Table 5, the total change in Δ, $\delta\Delta$, and in Ψ, $\delta\Psi$, after 2400 s of immersion in BSA1 are shown; the $\delta\Delta$ was approximately 0.8° for TiO_x, ZrO_x and NbO_x and 1.5° for TaO_x.

When the films were immersed in BSA0.1, the dynamic ellipsometry scans displayed a different behavior; a slower Ψ and Δ change-rate was observed for all the films, resulting in $\delta\Psi$ and $\delta\Delta$ values in the order of 0.2°.

The ellipsometry spectra of the metal oxide films after protein adsorption are shown in Fig. 4(a)–(d). Each figure includes the spectra of the film immersed in pure PBS, in BSA0.1 and in BSA1. The d_p and n_p of the adsorbed BSA layer from immersion in both BSA1 and BSA0.1 are listed in Table 5. For immersion in BSA0.1, d_p varied according to the film composition in a range between 5.3 and 14.2 nm, with the thickest BSA layer on TiO_x and the thinnest on TaO_x. Meanwhile, for immersion in BSA1, d_p varied in a range between 5.6 and 11 nm, again with the thickest BSA layer on TiO_x and the thinnest on TaO_x. Considering n_p as an indication of the BSA layer density, the densest layer was formed on the ZrO_x film and the least dense on TiO_x, independently of the BSA concentration in the solution. However, the protein layers formed were always less dense during immersion in the low concentration BSA solution.

In Fig. 5, the calculated surface mass density, Γ, of the adsorbed BSA layers are shown for each film and solution concentration. The Γ value differed among the different metal oxide films in the range of 1–0.31 μg/cm^2 and 0.6–0.22 μg/cm^2 for immersion in BSA1 and BSA0.1, respectively. The largest BSA adsorption occurs on ZrO_x and it decreased through TaO_x, NbO_x and TiO_x; this trend was observed independently of the protein concentration in the solution. However, the Γ value for BSA adsorption on the same metal oxide film was always lower for immersion in the solution with the lowest BSA concentration.

In Fig. 6, Γ is plotted against the corresponding RMS of the metal oxide film. A correlation between Γ and RMS was observed for BSA adsorption on the TaO_x, NbO_x and TiO_x films for both protein solutions; the rougher the surface, the larger the BSA adsorption. In Fig. 7, Γ is plotted against the polar component of the surface energy, γ^{AB} of the metal oxide films. Similarly, when only BSA adsorption on the TaO_x, NbO_x and TiO_x films was taken into account, a correlation between Γ and γ^{AB} were observed; the higher the γ^{AB}, the higher the Γ, independently of the protein solution. However, for BSA adsorption on ZrO_x, none of these correlations hold.

Table 5
Thickness, d_p, and refractive index, n_p, of adsorbed BSA layers after 2400 s of film immersion in protein solution and mean χ^2 obtained for the fitting of the SE data. The total change in the ellipsometric angles, $\delta\Delta$ and $\delta\Psi$, for immersion in BSA1 are shown.

Solution	BSA1					BSA0.1		
Film	d_p (nm)	n_p	χ^2	$\delta\Delta$ (°)	$\delta\Psi$ (°)	d_p (nm)	n_p	χ^2
TaO_x	5.6 ± 0.3	1.50	9.5	2.50	0.30	5.3 ± 0.2	1.49	10.5
NbO_x	8.0 ± 0.7	1.42	9.8	0.80	0.30	10.3 ± 0.3	1.40	10.0
TiO_x	11 ± 0.6	1.39	1.4	0.70	0.25	14.2 ± 2.0	1.38	2.4
ZrO_x	9.8 ± 0.9	1.52	3.6	0.80	0.45	6.9 ± 0.8	1.51	4.2

4. Discussion

In the present study the BSA adsorption on films of stoichiometric Ta, Nb, Ti and Zr oxides was studied. The films were amorphous except for the ZrO_x which showed to be partially crystalline. All the films were deposited under the same deposition conditions and on the same substrates; nevertheless, their R_a and RMS were significantly different ($p < 0.15$), Table 2. Thus, the observed differences in the surface roughness among the different metal oxide films can be mainly attributed to their different chemical compositions and structure.

The wettability properties of a surface can be characterized by their water contact angle, θ_w. A widespread definition is that an hydrophilic surface can be defined as the one presenting a $\theta_w > 90°$; however, according to a more biological definition the hydrophobic character can be considered for surfaces with $\theta_w > 68.2 \pm 5.7°$ [25]. According to this, the TaO_x, NbO_x and TiO_x films can be considered as hydrophilic but close to the hydrophobic–hydrophilic limit, and the ZrO_x film, ($\theta_w = 82 \pm 2.7°$), can be considered as hydrophobic. The films did not present significant differences in terms of their total surface energy, $\gamma^{LW/AB}$. However, the contributions of the polar, γ^{AB} and non-polar, γ^{LW}, components to the total energy are different in each metal oxide film. The contribution of γ^{AB} decreased from TaO_x with the strongest polar character, $\gamma^{AB} = 63\%$ of $\gamma^{LW/AB}$, towards NbO_x, TiO_x and ZrO_x with the weakest polar character, $\gamma^{AB} = 7\%$ of $\gamma^{LW/AB}$.

4.1. BSA adsorption kinetics

BSA adsorption from immersion in BSA1 occurred on all the metal oxide films showing a time dependent rate of adsorption. At the first 120s, the BSA adsorption rate, evaluated as the change-rate in Ψ and Δ, is in a very fast regime; as immersion time increased the adsorption rate rapidly decreased. However, it remained always positive implying that no evident BSA desorption occurred within this time framework. The observed BSA adsorption dynamic behavior is in agreement with in situ dynamic studies of protein adsorption on different surfaces [22,26–32] and agrees with theoretical studies. Theoretically, the protein adsorption rate is quite fast at the beginning of immersion due to an adsorption process dominated by the time that it takes a protein to reach a critical distance to the surface; then, the adsorption rate reaches

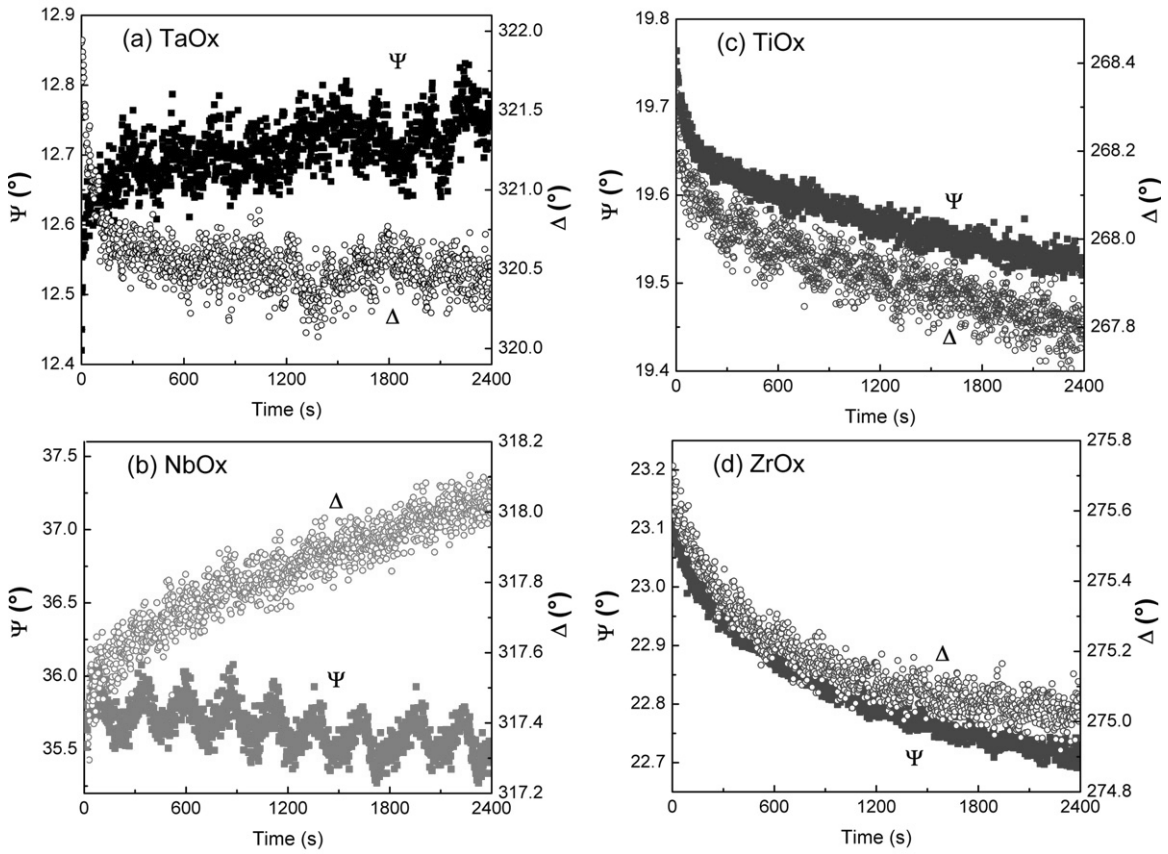

Fig. 3. Ellipsometry dynamic scans acquired at 3 eV recorded in situ on the (a) TaO_x, (b) NbO_x, (c) TiO_x, and (d) ZrO_x films for 2400 s of films immersion in BSA1.

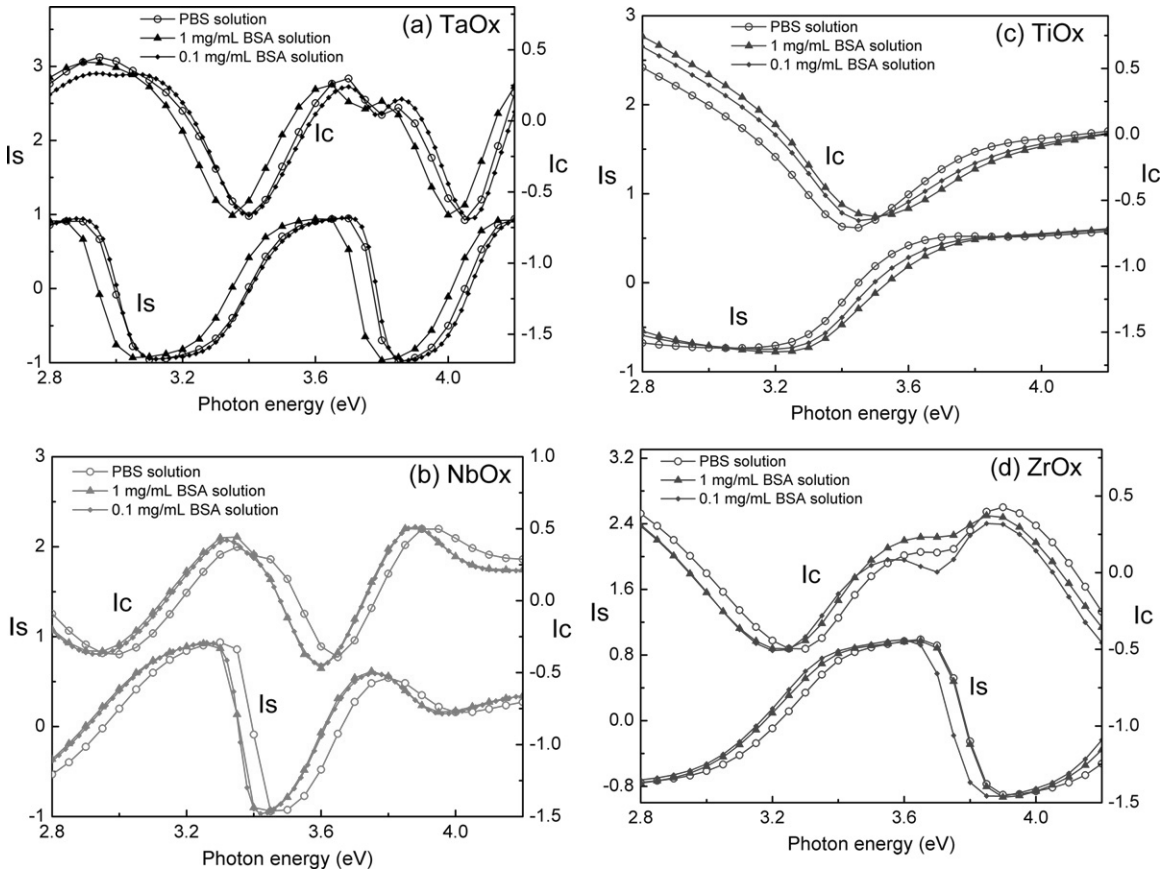

Fig. 4. Ellipsometry spectra measured in situ on the (a) TaO_x, (b) NbO_x, (c) TiO_x and (d) ZrO_x films immersed in PBS solution and after 2400 s of immersion in BSA1 solution and in BSA0.1 solution. Only the energy region from 2.8 to 4.2 eV is shown for better clarity in the spectra.

a maximum within the first minutes of immersion when the repulsion forces between the adsorbed proteins and the ones approaching becomes the dominant process and finally, a very slow adsorption regime is reached [33].

It has also been proposed that the 1process of removing adsorbed water molecules and hydrated ions from the surface contributes to an energy barrier that proteins have to overcome before being adsorbed [34]. In the present study, the influence of this process was more evident when the BSA concentration in the immersion solution was lowered (BSA0.1). In this case, the change rate in Ψ and Δ drastically decreased compared to the change rate observed for immersion in the most concentrated solution (BSA1), indicating a slower BSA adsorption rate for immersion in BSA0.1. The observation of a lower adsorption rate when protein concentration in the immersion solution is lowered is in agreement with previous protein adsorption studies [32,35,36]. A more diluted

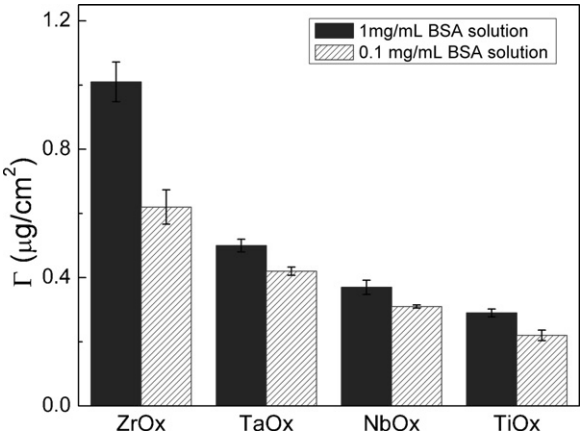

Fig. 5. Surface mass density, Γ, of the BSA layer adsorbed on the ZrO_x, TaO_x, NbO_x and TiO_x films, after 2400 s of immersion in BSA1 solution and in BSA0.1 solution, measured by in situ SE.

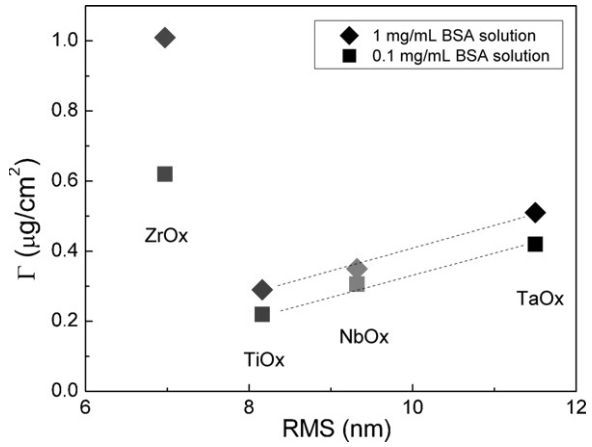

Fig. 6. Surface mass density, Γ, of the adsorbed BSA layer on the ZrO_x, TaO_x, NbO_x and TiO_x films, after 2400 s of immersion in BSA1 solution and in BSA0.1 solution, measured by in situ SE plot against the metal oxide thin film RMS roughness values. The lines in the graph do not represent a mathematical correlation among data points and are only presented as a visual aid.

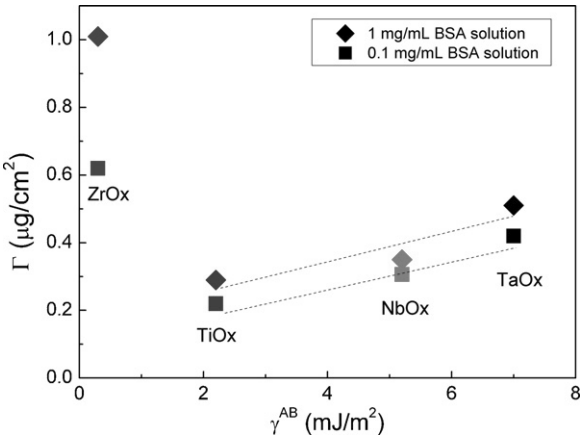

Fig. 7. Surface mass density, Γ, of the adsorbed BSA layer on the ZrO_x, TaO_x, NbO_x and TiO_x films after 2400 s of immersion in BSA1 solution and in BSA0.1 solution, measured by in situ SE plot against the value of the polar component of the total surface energy, γ^{AB}, of the metal oxide thin films. The lines in the graph do not represent a mathematical correlation among data points and are only presented as a visual aid.

solution has a smaller protein to water-ions ratio, meaning that the process of removing water and ions from the surface becomes more relevant for protein adsorption [7,25,34]; the process of removing water and ions is a slow process which consequently slows down the protein adsorption rate.

4.2. Adsorbed BSA layer

The Γ values in Fig. 5 showed that the quantity of mass adsorbed within the protein layer was dependent on the composition and surface properties of the metal oxide films and it was also dependent on the protein concentration in the immersion solution. The Γ values of the adsorbed BSA layers were always lower for immersion in the solution with the lowest BSA concentration, in agreement with the observations from the adsorption kinetics. The thickness and refractive index of the adsorbed BSA layers were different on the different metal oxide films, Table 5, even when immersion in the same protein solution is compared. This implies that the spatial orientation and packing of the BSA molecules within the adsorbed layer depend on the metal oxide film properties. Thicknesses of the BSA layers were in the range of 5.6–11 nm (immersion in BSA1) and 5.3–14.2 nm (immersion in BSA0.1). On previous BSA adsorption studies [30,37–39], it has been reported that d_p values between 4 and 14 nm might correspond to BSA molecules adsorbed with its long axis perpendicular to the surface, "standing-up", where the difference in thickness can be explained by different extents of spreading of the protein molecules. This suggestion is supported by the fact that the BSA is a soft protein that easily undergoes denaturation upon adsorption and thus, it easily spread over the surface upon adsorption [37,38]. According to the observed d_p values in the present study, the adsorbed protein layers can be suggested as formed by standing-up BSA molecules spread to different extents. The extent of spreading seems to be related to the film composition and BSA concentration in the immersion solution, but no clear trends can be defined.

The Γ of the BSA layers on TaO_x, NbO_x and TiO_x were in the range between 0.29 μg/cm² to 0.51 μg/cm² and 0.22 μg/cm² to 0.42 μg/cm² for immersion in BSA1 and BSA0.1, respectively. The Γ value calculated for a full monolayer of no-spread "side-on" (adsorbed with its long axis parallel to the surface, $d_p \sim 4$ nm) BSA molecules is ~0.19 μg/cm², and the corresponding Γ value for a full monolayer of no-spread "standing-up" BSA molecules ($d_p \sim 14$ nm) is ~0.70 μg/cm² [35,40]. Thus, the estimated Γ values for TaO_x, NbO_x and TiO_x films are in agreement with adsorbed layers of "standing-up" BSA molecules spread to different extents, in correspondence with the explanation given for the protein layer thicknesses. However, the results for the ZrO_x film are different; for immersion in BSA0.1, the Γ value, 0.62 μg/cm², suggests a full monolayer of almost no-spread "standing-up" BSA molecules, but the d_p value, 6.9 nm, is much lower than the expected value of 14 nm, as discussed above. Adsorbed BSA amounts of around 0.6 μg/cm² have been also found for BSA adsorption on powdered ZrO_2 [41]. On the other hand, the BSA layer adsorbed on ZrO_x from immersion in BSA1 showed a Γ value much larger than the expected for a full monolayer of no-spread "standing-up" BSA molecules (0.7 μg/cm²). According to the d_p value of this protein layer, 9.8 nm, then it could be explained by the adsorption of more than one layer of either "side-on" or widespread "standing-up" BSA molecules. The high n_p value of this protein layer, 1.52, also indicates multilayer adsorption, according to a previous study of albumin–anti-albumin mesothick multilayer precipitation on hydrophobic Si surfaces [42], where a maximum refractive index of 1.53 was determined.

4.3. Correlations between films surface properties and BSA adsorption

Different surface properties are known to influence protein adsorption on solid surfaces; however, no general rules have been reached in terms of such influences. In this work, for the amorphous and hydrophilic TaO_x, NbO_x and TiO_x films, a quasi-linear increase in the protein layer surface mass density with the RMS roughness of the film was observed, Fig. 6; independently of the protein concentration in the immersion solution. However, BSA adsorption on the partially nanocrystalline and hydrophobic ZrO_x film was notably larger even though the ZrO_x RMS roughness was lower than for TaO_x and NbO_x. The observed correlation between RMS and Γ for BSA adsorption on TaO_x, NbO_x and TiO_x could be macroscopically explained by a larger available surface area in the same two-dimensional space in a rougher surface; however, it does not necessarily imply that this macroscopic correlation would hold if the adsorption were normalized to the available surface area. Whether the correlation would hold or not will depend on other physicochemical properties influencing protein adsorption. The fact that BSA adsorption clearly increased on the ZrO_x film despite its RMS value is an indication of other physicochemical surface properties playing an important role in BSA adsorption.

A similar trend can be observed in Fig. 7, where Γ is plotted against the polar component of the total surface energy, γ^{AB}. There was an increment in Γ with the increment of γ^{AB}, when protein adsorption on the hydrophilic surfaces (TaO_x, NbO_x and TiO_x) is compared. However, BSA adsorption on ZrO_x did not fit into the same trend with the highest adsorption occurring on it despite ZrO_x being the surface with the lowest γ^{AB}. The largest BSA adsorption observed on ZrO_x may be a consequence of its hydrophobic character, in agreement with previous reports showing larger albumin adsorption on hydrophobic surfaces compared to adsorption on hydrophilic surfaces [9,11].

Protein adsorption on solid surfaces is a complex process that involves many promoting– or discouraging–adsorption interactions that can be generally summarized in three processes according to Haynes and Norde [38]: (a) partial dehydration of protein and surface, (b) redistribution of charged groups in the solid–liquid interface and (c) conformational changes in the protein molecule; which one of these processes will drive protein adsorption depends on the nature of the surface, the protein and the liquid medium. In water solvents at pH = 7.0, BSA folded

structure is such that the hydrophobic residues are preferentially located towards the core of the molecule; however, 40–50% of its accessible surface is still occupied by hydrophobic groups [38]. Thus, in the case of BSA adsorption on ZrO_x, both the surface and the BSA molecules have certain hydrophobic character. Then, a notoriously larger BSA adsorption occurring on the hydrophobic film, ZrO_x, compared to adsorption on the hydrophilic films could be explained assuming that the dehydration process is the main controlling step in the adsorption process; since dehydration becomes thermodynamically favorable when the surface and the adsorbate have a hydrophobic character [25,43]. On the opposite, the dehydration of a hydrophilic surface implies an energetic barrier. In agreement with the present study, an adsorption process highly influenced by the hydrophobic character of the substrate and where electrostatic interactions play a minor role has been also suggested for BSA adsorption on powdered ZrO_2 and phosphated ZrO_2 [44].

In the case when hydrophobicity is not a variable, such as TaO_x, NbO_x and TiO_x, the adsorption process is most probably controlled by a different mechanism; charge interactions and protein conformational changes. At pH around 7, the BSA molecule posses an overall negative charge [14]. Then, the largest BSA adsorption being observed on the surface with the largest γ^{AB}, TaO_x, indicates that the electrostatic interactions between the surface and the BSA molecules play an important role. A BSA adsorption process driven by electrostatic interactions on Nb_2O_5 and Ta_2O_5 has also been suggested by previous reports [45–47]. The other mechanism associated to BSA adsorption on the hydrophilic films could be the conformational changes of proteins upon adsorption, in agreement with previous studies showing that BSA easily undergo denaturation (conformational changes) on hydrophilic surfaces [37,48]. Indeed, in order to undergo conformational changes more easily upon adsorption, a larger adsorption area is required; which would be also in agreement with the largest BSA adsorption observed on the roughest film, TaO_x; there is a larger available area in the same 2-dimensional space in a rougher surface.

A large BSA adsorption might be desirable for biomaterials since the adsorbed BSA layer may act as a protective layer. However, different biological applications require different material–protein interactions; i.e. a non-fouling surfaces are needed for contact lenses, fibronectin adsorption is desirable for orthopedic implants, fibrinogen adsorption is relevant for materials where plasmatic coagulation is important, etc. [9,11,49–51]. Furthermore, generalized correlations among physicochemical surface properties and protein adsorption applicable to a variety of materials cannot be established yet; further studies using different proteins or mixed proteins solutions, studying a wider range of physicochemical surface properties, exploring different aspects of the adsorbed protein layers are needed in order to find those generalized correlations, which ultimately would enable us to establish clear directions to correlate protein adsorption to biocompatibility.

5. Conclusions

In this work, Ta_2O_5, Nb_2O_5, TiO_2 and ZrO_2 films were used as sample surfaces to study BSA adsorption from immersion in two solutions with different protein concentration. The BSA adsorption was followed in situ by dynamic ellipsometry and the adsorbed BSA layers after 2400 s of immersion were characterized by spectroscopic ellipsometry. The BSA adsorption rate decreased as protein concentration in the solution decreased. Different amounts of BSA were adsorbed on the different metal oxide films. The wettability of the films seems to have a strong influence on the BSA adsorption, which was significantly increased for adsorption on the hydrophobic film, ZrO_2.

In the case of adsorption on the films with a slightly hydrophilic character, TaO_x, NbO_x and TiO_x, BSA adsorption seems to be largely influenced by the electrostatic interactions. Correlations between the RMS and the γ^{AB} values of the films and the surface mass density, Γ, of the adsorbed BSA layer were observed. The larger the γ^{AB} or the RMS of the film, the larger the Γ of the adsorbed BSA layer.

Acknowledgements

The financial support from the CONACyT through the postdoctoral fellowship for Dr. P. Silva-Bermudez is gratefully acknowledged. Financial support from CONACYT project 152995 is gratefully acknowledged. Special thanks to Lazaro Huerta Arcos and Adriana Tejeda Cruz for technical assistance.

References

[1] J. Black, Clin. Mater. 16 (1994) 167–173.
[2] E. Eisenbarth, D. Velten, J. Breme, Biomol. Eng. 24 (2007) 27–32.
[3] S.O. Koutayas, T. Vagkopoulou, S. Pelekanos, P. Koidis, J.R. Strub, Eur. J. Esthet. Dent. 4 (2009) 348–380.
[4] R. Gunzel, S. Mandl, E. Richter, A. Liu, B.Y. Tang, P.K. Chu, Surf. Coat. Technol. 119 (1999) 1107–1110.
[5] A. Ochsenbein, F. Chai, S. Winter, M. Traisnel, J. Breme, H.F. Hildebrand, Acta Biomater. 4 (2008) 1506–1517.
[6] T. Vagkopoulou, S.O. Koutayas, P. Koidis, J.R. Strub, Eur. J. Esthet. Dent. 4 (2009) 130–151.
[7] B. Kasemo, J. Lausmaa, Environ. Health Perspect. 102 (1994) 41–45.
[8] B. Kasemo, J. Lausmaa, Mater. Sci. Eng. C: Biomim. 1 (1994) 115–119.
[9] C. Werner, M.F. Maitz, C. Sperling, J. Mater. Chem. 17 (2007) 3376–3384.
[10] K. Anselme, L. Ploux, A. Ponche, J. Adhes. Sci. Technol. 24 (2010) 831–852.
[11] C.J. Wilson, R.E. Clegg, D.I. Leavesley, M.J. Pearcy, Tissue Eng. 11 (2005) 1–18.
[12] P. Parhi, A. Golas, E.A. Vogler, J. Adhes. Sci. Technol. 24 (2010) 853–888.
[13] B. Blomback, L.A. Hanson, Plasma Proteins, John Wiley & Sons, Chichester, 1976, pp. 43-54.
[14] T.J. Peters, All about albumin: biochemistry, in: Genetics and Medical Applications, Academic Press, San Diego, CA, 1996.
[15] A.F. Stalder, G. Kulik, D. Sage, L. Barbieri, P. Hoffmann, Colloid Surface A 286 (2006) 92–103.
[16] C.J. Vanoss, R.J. Good, M.K. Chaudhury, Langmuir 4 (1988) 884–891.
[17] S.Y. Kim, Appl. Opt. 35 (1996) 6703–6707.
[18] E. Franke, M. Schubert, C.L. Trimble, M.J. DeVries, J.A. Woollam, Thin Solid Films 388 (2001) 283–289.
[19] R.E. Klinger, C.K. Carniglia, Appl. Opt. 24 (1985) 3184–3187.
[20] K.P.S.S. Hembram, G. Dutta, U.V. Waghmare, G.M. Raoa, Physica B 399 (2007) 21–26.
[21] B. Karunagaran, R.T.R. Kumar, C. Viswanathan, D. Mangalaraj, S.K. Narayandass, G.M. Rao, Cryst. Res. Technol. 38 (2003) 773–778.
[22] T. Berlind, P. Tengvall, L. Hultman, H. Arwin, Acta Biomater. 7 (2011) 1369–1378.
[23] R.A. Synowicki, G.K. Pribil, G. Cooney, C.M. Herzinger, S.E. Green, R.H. French, M.K. Yang, J.H. Burnett, S. Kaplan, J. Vac. Sci. Technol. B 22 (2004) 3450–3453.
[24] J.A. Defeijter, J. Benjamins, F.A. Veer, Biopolymers 17 (1978) 1759–1772.
[25] E.A. Vogler, J. Biomater. Sci. Polym. E 10 (1999) 1015–1045.
[26] R. Seitz, R. Brings, R. Geiger, Appl. Surf. Sci. 252 (2005) 154–157.
[27] I. Otsuka, M. Yaoita, S. Nagashima, M. Higano, Electrochim. Acta 50 (2005) 4861–4867.
[28] F. Hook, J. Voros, M. Rodahl, R. Kurrat, P. Boni, J.J. Ramsden, M. Textor, N.D. Spencer, P. Tengvall, J. Gold, B. Kasemo, Colloid Surf. B 24 (2002) 155–170.
[29] H. Arwin, Thin Solid Films 377 (2000) 48–56.
[30] N.J. Freeman, L.L. Peel, M.J. Swann, G.H. Cross, A. Reeves, S. Brand, J.R. Lu, J. Phys. Condens. Mater. 16 (2004) S2493–S2496.
[31] A. Tsargorodskaya, A.V. Nabok, A.K. Ray, Nanotechnology 15 (2004) 703–709.
[32] S.K. Pattanayek, L.M. Pandey, Appl. Surf. Sci. 257 (2011) 4731–4737.
[33] F. Fang, I. Szleifer, Biophys. J. 80 (2001) 2568–2589.
[34] N. Barnthip, H. Noh, E. Leibner, E.A. Vogler, Biomaterials 29 (2008) 3062–3074.
[35] S.J. McClellan, E.I. Franses, Colloid Surf. B 28 (2003) 63–75.
[36] S.J. McClellan, E.I. Franses, Colloid Surf. A 260 (2005) 265–275.
[37] W. Norde, C.E. Giacomelli, Macromol. Symp. 145 (1999) 125–136.
[38] C.A. Haynes, W. Norde, J. Colloid Interface Sci. 169 (1995) 313–328.
[39] P. Bertrand, Appl. Surf. Sci. 252 (2006) 6986–6991.
[40] T.M. Byrne, L. Lohstreter, M.J. Filiaggi, Z.J. Bai, J.R. Dahn, Surf. Sci. 603 (2009) 992–1001.
[41] V. Pachova, M. Ferrando, C. Guell, F. Lopez, J. Food Sci. 67 (2002) 2118–2121.
[42] J. Benesch, A. Askendal, P. Tengvall, J. Colloid Interface Sci. 249 (2002) 84–90.

[43] R.D. Tilton, C.R. Robertson, A.P. Gast, Langmuir 7 (1991) 2710–2718.
[44] B. Putman, P. VanderMeeren, D. Thierens, Colloid Surf. A 121 (1997) 81–88.
[45] R. Michel, S. Pasche, M. Textor, D.G. Castner, Langmuir 21 (2005) 12327–12332.
[46] S. Pasche, S.M. De Paul, J. Voros, N.D. Spencer, M. Textor, Langmuir 19 (2003) 9216–9225.
[47] N.P. Huang, R. Michel, J. Voros, M. Textor, R. Hofer, A. Rossi, D.L. Elbert, J.A. Hubbell, N.D. Spencer, Langmuir 17 (2001) 489–498.
[48] W. Norde, J.P. Favier, Colloid Surf. 64 (1992) 87–93.
[49] D. Bozukova, C. Pagnoulle, R. Jerome, C. Jerome, Mater. Sci. Eng. R 69 (2010) 63–83.
[50] J. Ramsden, Biomedical Surfaces, Artech House, Norwood, MA, 2008.
[51] T.S. Tsapikouni, Y.F. Missirlis, Mater. Sci. Eng. B: Adv. 152 (2008) 2–7.